Adsorption of Ni^{2+} Ions onto NaX and NaY Zeolites: Equilibrium, Kinetics, Intra Crystalline Diffusion and Thermodynamic Studies

Ferhat, Djawad; Nibou, Djamel*+; Elhadj, Mekatel; Amokrane, Samira

Laboratory of Materials Technology, University of Science and Technology Houari Boumediene, B.P. 32, El-Alia, Bab-Ezzouar, Algiers, ALGERIA

ABSTRACT: *This paper focus on intra crystalline diffusion of Ni^{2+} ions onto NaX and NaY zeolites. The zeolites are obtained by hydrothermal synthesis method. The samples were characterized by several techniques: X-Ray Diffraction (XRD), Scanning Electron Microscopy (SEM) coupled with Energy Dispersive Spectroscopy (EDS) and InfraRed Spectroscopy (FT-IR). Physical parameters such as pH solution (2 - 7), adsorbent dose (0.25 - 2 g/L), initial concentration of Ni (II) ions (50 - 200 mg/L) and temperature (298 - 323 K) are optimized. The maximum uptake is 99% and 97% for NaX and NaY zeolite respectively under the optimum conditions: pH ∼ 7 and adsorbent dose of 1 g/L for initial concentration of 50 mg/L at 298 K. The best interpretation of the experimental data is obtained by the Langmuir isotherm with a maximum adsorption capacity of 111.85 and 77.57 mg/g for NaX and NaY respectively. The results show that the kinetic data for both zeolites follow the pseudo second order model, indicating the presence of physical adsorption. The free energy (ΔG^o), enthalpy (ΔH^o) and entropy ($\Delta S°$) are evaluated. The process has proved its spontaneous and endothermic. Diffusion mechanisms of Ni (II) ions adsorption onto NaX and NaY has shown that intra particle diffusion is the limiting step of the process. The NaX and NaY have been applied to wastewater from the Algerian industrial zone in order to eliminate the Ni^{2+} effluents using the optimal parameters. It has been found that the Ni^{2+} ions removal yield was 77.81% for NaX and 83.86% for NaY.*

KEYWORDS: *Adsorption; Nickel ions; Zeolite; kinetic; diffusion; thermodynamic.*

INTRODUCTION

Nowadays, the problem of heavy metals is becoming more worrying, because they are difficult to eliminate such as the industrial wastewater, contained different types of heavy metal ions and organic pollutants, which may cause a serious environmental problems that can affect the public health. Many methods such as ion exchange, precipitation, membrane processes, ultra-filtration, electro dialysis and reverse osmosis have been performed for toxic metal ions and organic pollutants removal [1-5]. Among these processes, adsorption is one of the most efficient techniques owing to its various advantages such as high relatively easy regeneration,

** To whom correspondence should be addressed.*
+ E-mail: dnibou@yahoo.fr
1021-9986/2018/6/63-81 6/$/5.06

adsorption capacity, fast kinetics and the use of a large variety of adsorbent materials (zeolites, clays and biomasses) [6,7]. Zeolites are microporous materials, which have been extensively used in various applications, *e.g.* as catalysts, for separating and sorting various molecules, for water and air purification, including removal of radioactive contaminants, for harvesting waste heat and solar heat energy, for adsorption refrigeration, as detergents, *etc.* The growth of zeolites for environmental applications depends primarily on their physical properties and especially on the specific surface area [8-10]. The properties of extremely wide zeolites such as their hydrophilic and hydrophobic properties, high surface area, tunable chemical properties, high thermal stability and eco-friendly nature. Zeolites are microporous microcrystalline inorganic materials capable of adsorbing organic molecules [11]. The NaX and NaY Zeolites are suitable for adsorptions due to the high cation exchange capacity and the affinity for heavy metals as Ce^{3+}, La^{3+}, UO_2^{2+}, Co^{2+}, Sr^{2+}, Pb^{2+}, Tl^{+} [2], Zn^{2+} [6] and Cu^{2+} [12].

Moreover, the main contents of zeolites are aluminum and silicon oxides. They are an open structure with compensation charge cations as Na^{+} and K^{+}. Theses cations are readily exchangeable with other present in the solution [13]. Zeolite are classified into two major groups of natural and synthetic, X and Y are two most famous synthetic zeolites [14-18]. The Si/Al of NaX: 1<Si/Al<1,5 and NaY : Si/Al > 1,5 ratio directly influences the position and the number of the compensating cations on the type of crystal [19].

The kinetics of adsorption has also an important impact on the performance of the zeolites. The adsorption contains three phases of transfer of the zeolite and a reaction phase. The first represents the migration of the solute from the aqueous phase to the surface of the zeolite (external diffusion). The second related to intra-particle diffusion, and finally the surface chemical reaction between these functions of the zeolite and the metal ions [20-21]. Therefore, chemical exchange is slow comparing to other diffusion processes, which involve the determination step of the mechanism [6,22]. Several mathematical models describing a system of a particle at constant pressure and volume have been used by some authors in the literature [23-25]. They have assumed that the kinetic order of the chemical exchange is two and reported that the exchange process is characterized by a linear relationship between $1/(q_\infty-q_t)$ and t where q_∞ and q_t are the adsorption capacity at ∞ and at time t respectively. Contrary, other authors [26-28] have achieved the result that the variation of $\ln(1/q_\infty-q_t)$ in function time t should be linear if the chemical reaction is crucial, taking in consideration its approaches.

In the present work some characteristics of NaX and NaY zeolites are investigated by XRD, SEM, EDS and FT-IR techniques. Optimized parameters influencing the adsorption phenomenon as pH solution, zeolite dose, initial concentration of Ni^{2+} ions and the temperature are performed. In order to identify the adsorption mechanism, Langmuir, Freundlich and Temkin isotherms models are used. Kinetic studies using pseudo first-order, pseudo second-order and diffusion models are performed. We have focused on the use of models based on Fick laws during the analysis of the data obtained experimentally and for determining the step which describes the mechanism of the reaction. Thermodynamic parameters i.e. enthalpy of adsorption $\Delta H°$ entropy change $\Delta S°$ and Gibbs free energy $\Delta G°$ for the adsorption of Ni^{2+} ions onto NaX and NaY zeolites were examined. The obtained optimal parameters have been applied to wastewater from the industrial zone (West Algiers, Algeria).

EXPERIMENAL SECTION

The NaX and NaY were obtained by hydrothermal method as illustrated in the previous paper [6, 13]. All reagents used in the present study were analytical grade, $Ni(NO_3)_2{\cdot}6H_2O$ (98%) from Biochem chemopharma. The NaOH was from Fluka chimika. Both of HCl and KCl were from Sigma-Aldrich. In all experiments, we used distilled water, which is obtained by GFL 2008. The unit cells composition in dry basis of NaX and NaY were $Na_{81}(AlO_2)_{81}(SiO_2)_{111}$ and $Na_{51}(AlO_2)_{51}(SiO_2)_{141}$ corresponding to a CEC of 5.96 and 3.90 meq/g respectively. The surface areas of prepared NaX and NaY were 375 and 304 m^2/g.

Characterization

The morphological and physico-chemical properties of the samples were characterized by XRD (Panalytical X'Pert PRO, Germany, using CuKα radiation) at a scanning range 2θ from 5 to 50°. The surface morphology was observed by SEM (JEOL 6360, Japan) equipped with EDS. We use carbon to coat our samples with a thin film.

The FT-IR analysis was carried out using Perkin Elmer Spectrum equipment (Version 10.03.06, Germany). Surface area measurements were conducted using Micrometrics ASAP 2010 apparatus.

Batch adsorption

Batch adsorption experiments of Ni^{2+} ions were carried out in a double-walled Pyrex reactor of capacity 200 cm^3 whose temperature was regulated by a thermostat bath. Preparation of the Ni^{2+} solutions between (50–200 mg/L) were started by dilution of stock solution of (1000 mg/L). The effect of pH was studied in the range of 2 to 7 with optimized condition such as 0.2 g of adsorbent dropped in 200 mL of Ni^{2+} ions with (C_0=100 mg/L) in room temperature solution. We use NaOH (0.1 M) or HCl (0.1 M) to adjust our pH. The adsorption kinetics and isotherms of the solutions between (50–200 mg/L) have been performed at different temperatures (25, 30, 40, and 50 °C). The final Ni^{2+} concentration is determined using UV–Vis spectrophotometer (Optizen 2120 UV–Visible, Korea, maximum of wavelength is 465 nm) [1,29]. Using the following relationship, we calculated the removal percentage of Ni^{2+} ions.

$$\text{Removal of } Ni^{2+}(\%) = \frac{(C_i - C_e)}{C_i} \times 100 \qquad (1)$$

Where C_i and C_e are the initial and equilibrium Ni^{2+} concentrations (mg/L) respectively. The adsorption capacity of the samples, q_t (mg/g), were determined using the relationship:

$$q_t = \frac{(C_i - C_e)V}{C_i m} \qquad (2)$$

Where V is the volume of the Ni^{2+} solution and m is the weight of our adsorbent. The equilibrium constant K_c is given by [30].

$$K_c = \frac{(C_i - C_e)}{C_e} \qquad (3)$$

RESULTS AND DISCUSSION

Zeolite Characterization

X-ray diffraction studies

Fig. 1 (a, b) shows the XRD patterns of the NaX and NaY zeolites. The identification of the phases was done according to a standard file (JCPDS 00-012-0228) and reveal a cubic structure for both zeolites which promote better ions exchange [31]. The spectra show the presence of all the crystallization planes (hkl) of the NaX and NaY structures. On the other hand, the NaX sample exhibits a strong peak compared to those of NaY showing a good crystallinity.

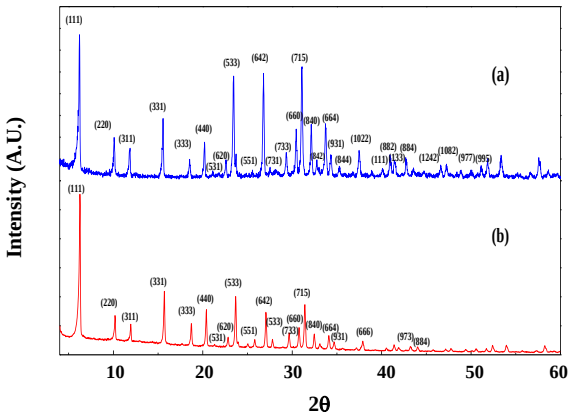

Fig. 1: XRD patterns of NaX (a) and NaY (b) zeolites.

The crystallite size was determined by the Scherrer Equation (4) [32-33]:

$$D = \frac{K\lambda}{\beta \cos\theta} \qquad (4)$$

Where K is usually 0.89 is the Scherrer constant, λ (1.54056 Å) is the wavelength of X-ray radiation, β is the peak full width at half maximum in radians and θ is the Bragg diffraction angle. The estimated values of grain size are 0.20-1.4 nm range for NaX and NaY zeolites.

SEM micrographs analysis

Fig. 2 shows the SEM micrographs of NaX (a) and NaY (b) with respective EDS analysis. The form of obtained particles seems to be cubic with clearly visible facets and with a homogeneous size distribution of about 10 and 5 µm respectively.

The EDS analysis shows the presence of the main essential elements of the NaX and NaY framework Si and Al and the compensation cations Na. From the results, the values of Si/Al atomic ratio of NaX and NaY samples are 1.28 and 2.63 respectively. It can be observed that the value of NaY ratio is superior to that NaX. These results are in good agreement with those cited in the bibliography [13,14]. The NaY ratio directly influences

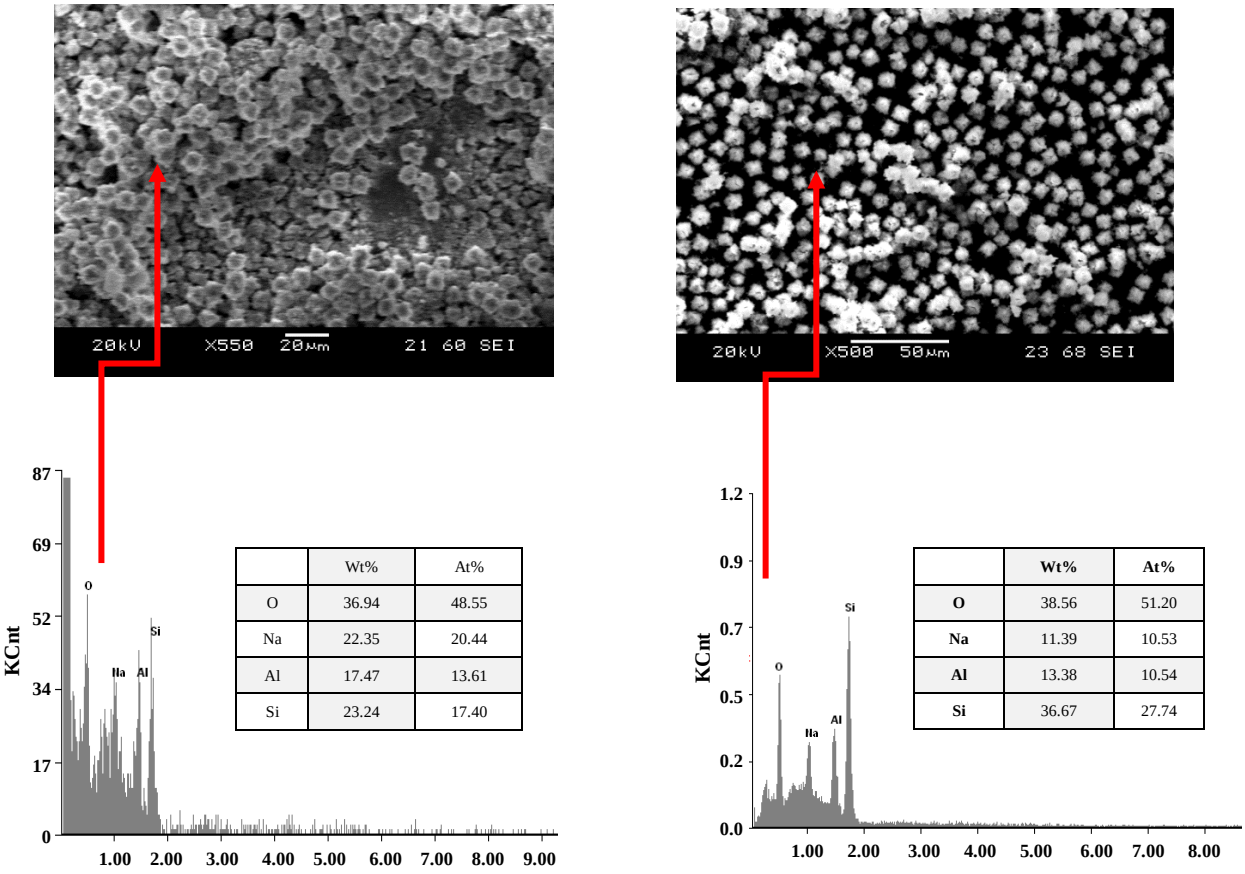

Fig. 2: SEM micrographs of NaX (a) and NaY (b) zeolites with respective EDS analysis.

the atomic percentage of the cations compensating (10.53) compared to the NaX sample (20.44) as shown in Fig 2.

FT-IR spectral analysis

The NaX and NaY samples were characterized by FT-IR to observe the absorption bands grouped in Table 1 and illustrated in Fig 3. In general, the vibration spectrum of the NaX and NaY zeolites consists of two types of bands. First bands due to the internal vibrations of the TO_4 (T = Si, Al) tetrahedra which constitute the primary unit of the structure [6,14]. They are not very sensitive to structural vibrations. Second bands corresponding to the vibrations of the TO_4 tetrahedra with respect to one another. They are obviously sensitive to the way in which the tetrahedra are both attached. The samples analyzed show bands at 1200 to 450 cm^{-1} which correspond to the vibrations of Si-O-Al, Si-O-Si, Si-O, and Al-O. Other absorption bands between 3800 to 3450 and 1600 cm^{-1} are also present and are attributed to the vibrations of the hydroxyl groups Si-OH and H_2O respectively [20,33,34,35].

Determination of zero point charge pHpzc of NaX and NaY zeolite

The pH at which the charge of the adsorbent surface is zero is referred to as the zero point of charge (pHpzc). The pH_{pzc} is one of the important parameters for discussion of pH effect. The pHpzc of NaX and NaY zeolite samples was determined by the method cited in [36-38]. KCl solution (0.001 M) was transferred to a series of Erlenmeyer flasks who are made up to exactly 50 mL. The initial pH of each flasks was adjusted by adding either HCl (0.1 M) or NaOH (0.1 M) to decrease

Table 1: Infrared absorption bands characteristic of NaX and NaY.

Type of bond	Frequencies (cm^{-1}) from Breck [14]	Frequencies (cm^{-1})	
		NaX	NaY
Asymmetric elongation Si-O-Al, Si-O-Si	1250-950	989	989
Symmetrical elongation Al-O	720-650	679	717
Vibration of tetrahedral vertices Si, Al-O	650-500	565	659
Symmetrical elongation Si-O-Al, Si-O-Si	820-750	755	788
Asymmetric elongation Si-O-Al	1150-1050	-	-

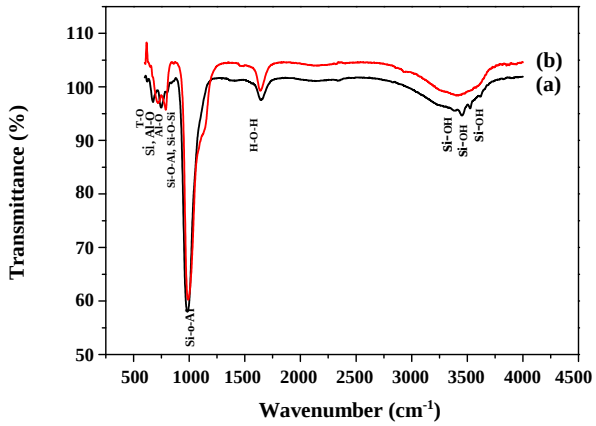

Fig. 3: FT-IR spectra of NaX (a) and NaY (b) zeolites.

or increase it respectively. 0.2 g of zeolite was added to each flask. After stirring 48 h, the suspensions were filtered and the final pH values of the supernatant liquid (pH_{final}) were recorded. The pH_{ZPC} is the point where the curve pH final versus pH initial crosses the line the axis of the bisectors. pH_{ZPC} of NaX and NaY zeolites was experimentally found to be at pH 8.0 and 7 respectively Fig. 4. At the solution pH values lower than pHpzc, the active sites of the adsorbent are protonated and have positive charge. However, at the pH values higher than the pHzpc, the surface charge of the adsorbent is negative.

Adsorption study

The pH of solution as parameter of control is used which powerfully affects the adsorption of Ni^{2+} ions on the adsorbent surface. The influence of pH has been studied between 2 until 8. Fig. 5 (a) shows a maximum removal of Ni^{2+} ions (91% NaX and 63% NaY) at pH ~ 7. At lower pH_s values the adsorbents have a net positive charge but a minimum elimination of Ni^{2+} ions is obtained at lower pH. Probably, it may be due to the electrostatic attractions between the positively charged adsorbent surface and the negatively functional groups charge located on Ni^{2+} [39-40].

The uptake of Ni^{2+} ions by NaX and NaY samples was fast at the beginning due to a larger surface area of adsorbent and gradually decreases with time until it reaches saturation. As we can see in Fig. 5 (b), the first stage is the faster until reaching 15 min. The second (15-120 min) is slower because of the saturation of active zeolite sites. The equilibrium which is the last step is due to the occupation of all actives sites.

The effect of NaX and NaY dosage of removal of Ni^{2+} ions at C_i = 100 mg/L was studied and filled in Fig. 5 (c). The adsorbent dose was varied from 0.25 to 2 g/L for each zeolite, keeping the concentration of metal ion fixed. Theoretically, increasing the adsorbent dose increases the adsorption and improve more metal ion elimination. The main reason that governs this supposition is the availability of more adsorption sites due to large surface area available for adsorption initially [41]. Fig. 5 c shows that high doses positively influence the adsorption removal of Ni^{2+} ions; this is attributed to the increased available sites with increasing the amount of the zeolite where the adsorption increases progressively to peak at 99.86% for NaX and 95.15% for NaY. From these results, it can be concluded that the best Ni^{2+} ions adsorption by NaX occurs for an optimal dose of 2 g/L.

Adsorption of Ni^{2+} ions on NaX and NaY is affected by the initial concentration at 25°C between 50 and 200 mg/L. Results mentioned in Fig. 5 (d) illustrated that the adsorption of Ni^{2+} decreased when the concentration of the solution increased. This indicates that less favorable sites occur when the concentration of solution achieving a maximum removal of 99.67 % and 97.40 % at 50 mg/L

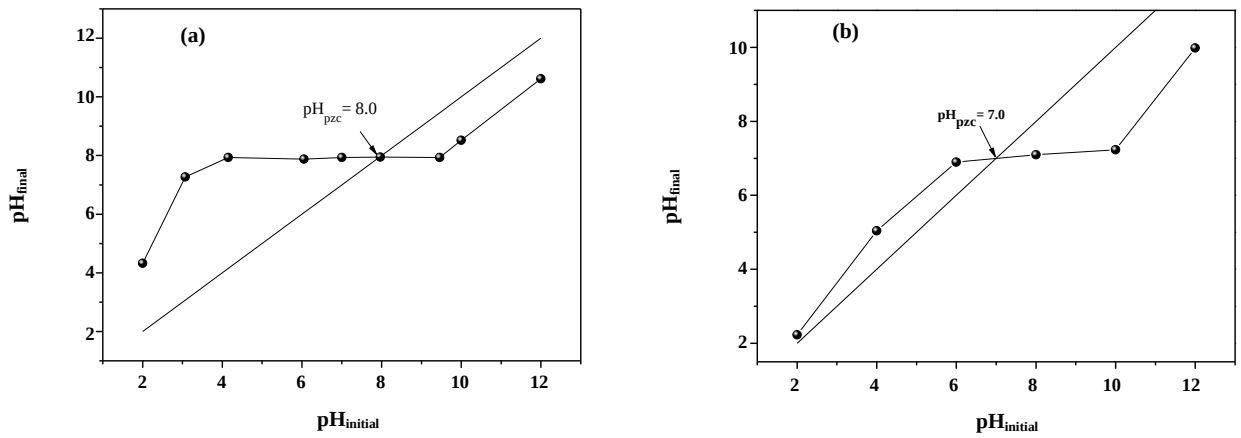

Fig. 4: Point of zero charge of NaX (a) and NaY (b) zeolites.

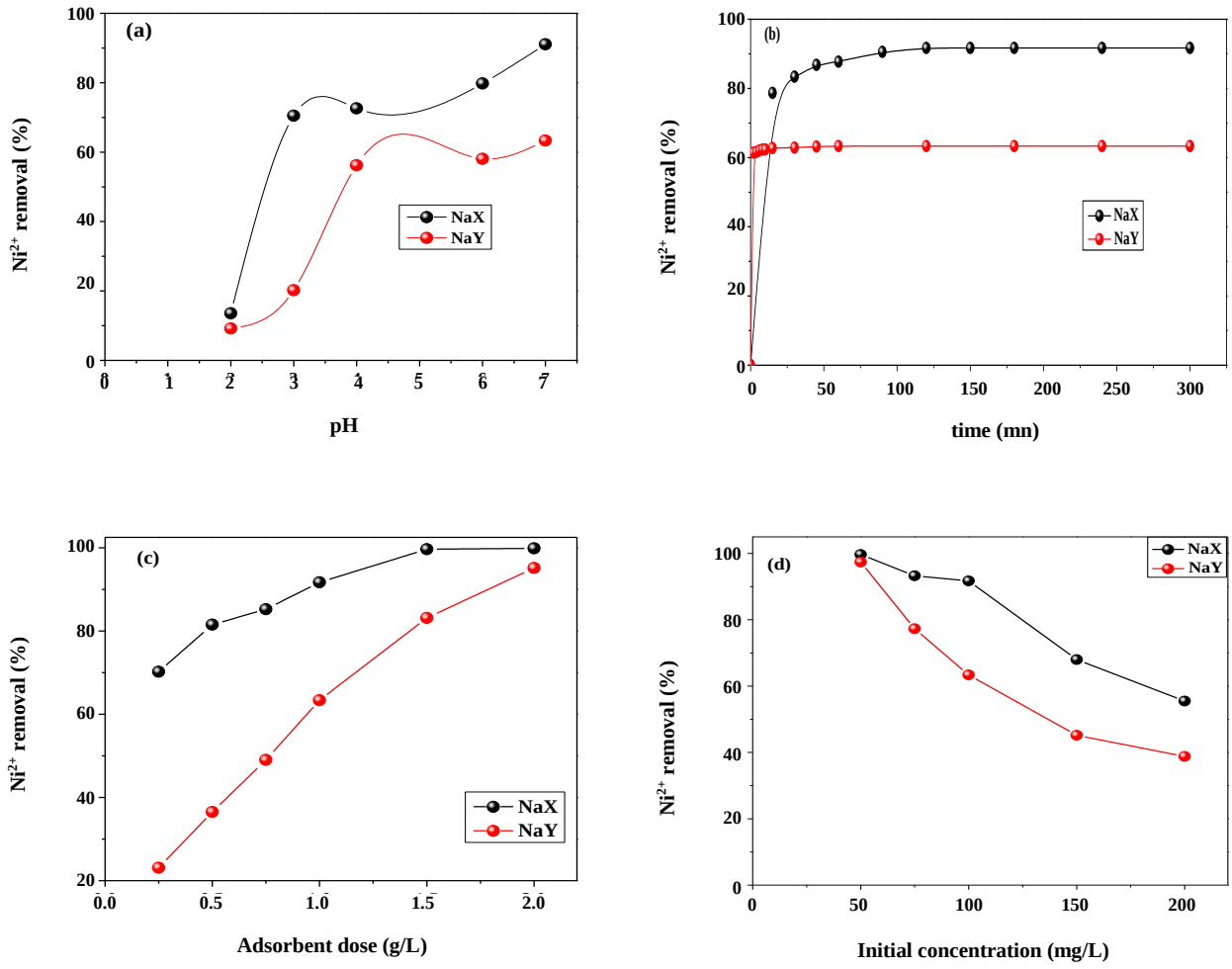

Fig. 5: Factors affecting Ni^{2+} ions adsorption onto NaX and NaY: (a) pH effect, (b) contact time, (c) adsorbent dose and (d) initial concentration effect.

Table 2: Results of the equilibrium isotherm models of NaX and NaY (pH ~7, C_i = [50 – 200 mg/L], adsorbent dose = 1 g/L and T = 298 K).

Model	Parameters	Value	
		NaX	NaY
Langmuir	q_m (mg/g)	111.85	77.57
	b (L/mg)	0.482	0.186
	R^2	0.9970	0.9864
Freundlich	K_F (L/g)	62.61	46.32
	1/n	0.128	0.093
	R^2	0.9490	0.9320
Temkin	k_T (L/mg)	783.38	3032.18
	b_T (J/mol)	254.53	440.19
	R^2	0.9103	0.8501

for NaX and NaY samples respectively. A minimum of removal of 60 and 40% at 200 mg/L was also obtained from the respective samples. This retention for low initial Ni^{2+} ions concentrations might be explained by the active sites available on the adsorbent. The increase of the Ni^{2+} ions concentration leads to a rapid saturation of active sites, resulting in a decreased removal efficiency [42-44].

Equilibrium isotherms

Three well-known models *Langmuir* [45], *Freundlich* [46] and *Temkin* [47-49] have been tested in this work. The Equations (5), (6) and (7) have been used for each model respectively.

$$\frac{C_e}{q_e} = \frac{1}{q_m b} + \frac{C_e}{q_m} \quad (5)$$

Where C_e is the equilibrium concentration of Ni^{2+} (mg/L) and q_e is the amount of adsorbed Ni^{2+} (mg/g). The monolayer adsorption capacity q_m (mg/g) and the Langmuir constant related to the free adsorption energy *b* (L/mg) (Table 2) were evaluated from the slope and intercept of the linear plots of C_e/q_e versus C_e respectively (Fig. 6 (a)).

$$\ln q_e = \ln K_F = \frac{1}{n} \ln C_e \quad (6)$$

Where K_F (mg/g) and *n* are the Freundlich constants related to adsorption capacity and adsorption intensity respectively. The values of K_F and *n* (Table 2) were determined from the intercept and slope of the linear plot of ln q_e versus ln C_e (Fig. 6 (b)).

$$q_e = \frac{RT}{b_T} \ln K_T + \frac{RT}{b_T} \ln C_e \quad (7)$$

Where k_T (L/mg), *R* (8.314 J/mol k), *T* (K) and b_T (J/mol) are the Temkin constants related to the binding equilibrium isotherm, universal gas constant, the temperature and the variation of adsorption energy respectively. The constants were determined from the slope and the intercept (Fig. 6 (c)).

The adsorption isotherms of Ni^{2+} ions onto NaX and NaY are tested. As illustrated in Table 2, Langmuir isotherm was more suitable than the Freundlich and Temkin isotherms. In the most cases, the correlation coefficients were higher, indicating the applicability of monolayer coverage of the Ni^{2+} on the surface of adsorbents. The Langmuir model describes the sorption data with a correlation factor R^2 values greater than 0.997. According to the saturated monolayer sorption capacity q_m and b, the NaX adsorbs better compared to NaY. On the other hand, the equilibrium data were analyzed using Freundlich and Temkin isotherm models and R^2 values were estimated as shown in Table 2. The values of 1/n for NaX and NaY were inferior to 1, indicating that adsorption capacity is only slightly suppressed.

To confirm the performance of the Ni^{2+} ions adsorption onto NaX and NaY, the separation factor R_L was calculated using the following Eq. (8).

$$R_L = \frac{1}{1 + b C_i} \quad (8)$$

Where *b* (L/mg) constant Langmuir. The R_L value indicates the nature of adsorption process. In fact,

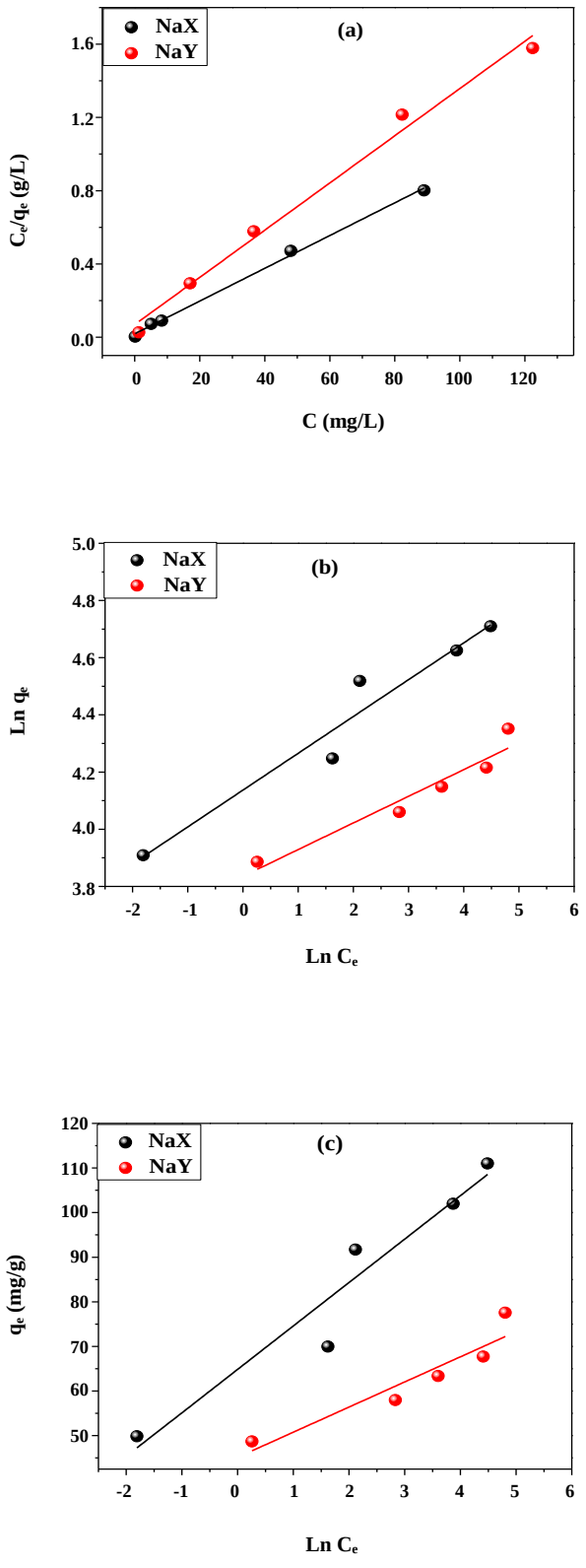

Fig. 6: Langmuir (a) Freundlich (b) and Temkin (c) isotherms for adsorption of Ni^{2+} ions onto NaX and NaY (pH ~7, C_i = [50 – 200 mg/L], adsorbent dose = 1 g/L and T = 298 K).

the isotherm is unfavorable when $R_L > 1$, linear when $R_L = 1$, favorable when $R_L < 1$ and irreversible when $R_L = 0$ [6, 24]. The values of the R_L factor at different initial concentrations are presented in the Table 3. The R_L values for the adsorption of Ni^{2+} ions are inferior to 1, demonstrating that the adsorption process is favorable.

Adsorption kinetics

In this part of the study, the mechanism of Ni^{2+} ions adsorption onto NaX and NaY was defined by a pseudo-first-order, pseudo-second-order and intra-particle diffusion models.

A pseudo-first-order Lagergren model is based on the hypothesis that the rate of adsorbate seizing the adsorption sites is proportional to the amount of intake adsorption sites .It can be expressed by Eq. (9).

$$\ln(q_e - q_t) = \ln q_e - k_1 t \quad (9)$$

Where q_e is the adsorption capacity at equilibrium (mg/g); q_t is the adsorption capacity (mg/g) at the time t and k_1 is the first order rate constant (1/min). The values of kinetic constants q_e and k_1 are defined experimentally from the slop and the intercept of the linear plot of ln ($q_e - q_t$) versus t, respectively (Fig.7 and Fig.8).

The pseudo-second-order model was deduced, based on the hypothesis that the sorbent absorbed the adsorbate chemically [50]. It can be expressed by Eq (10).

$$\frac{t}{q_t} = \frac{1}{k_2 q_e^2} + \frac{t}{q_t} t \quad (10)$$

Where k_2 is the second order rate constant (g/mg min). The values of kinetic constants q_e and k_2 are defined experimentally from the slope and intercept of the linear plot of t/q_t versus t, respectively (Fig.9 and Fig.10).

In order to confirm if Ni^{2+} ions adsorption into the pores of NaX and NaY is dominated by particle diffusion, the empirical data were analyzed using the intra-particle diffusion model [51]. The results showed in Table 4 suggest that pseudo-second order model is the most reliable to determine the order of the adsorption kinetics of Ni^{2+} ions onto NaX and NaY which represents a good correlation coefficient ($R^2 > 0.999$). Similarly, we note that the values of q_e calculated by the pseudo-second order model is very close to those determined experimentally which further justifies that the kinetics of

Table 3: Dimensionless factor R_L of the adsorption of the Ni^{2+} ions onto NaX and NaY.

Dimensionless factor (R_L)		
C_o (mg/L)	NaX	NaY
50	0.0398	0.0970
75	0.0269	0.0668
100	0.0203	0.0510
150	0.0136	0.0346
200	0.0103	0.0261

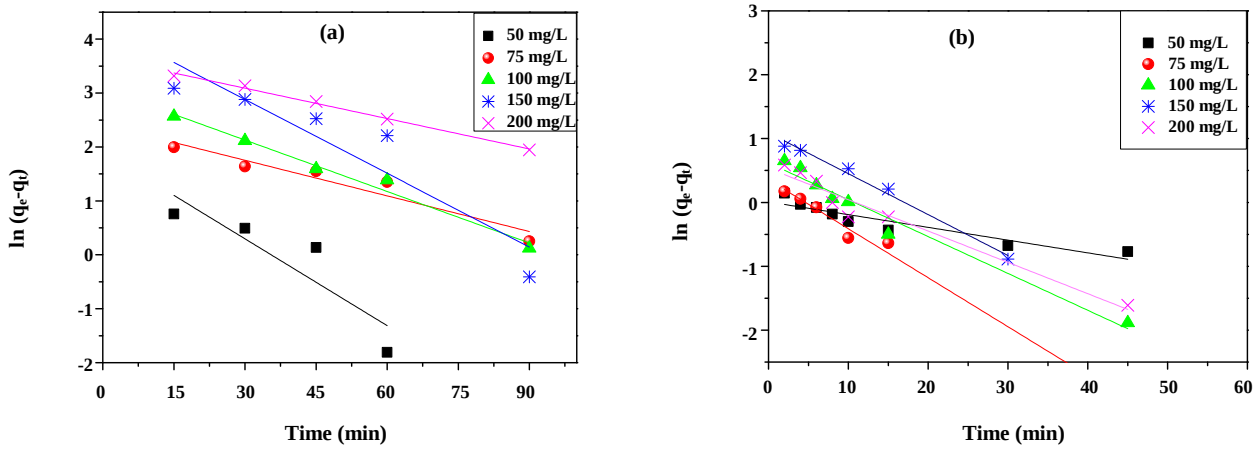

Fig. 7: Application of the Pseudo-First Order kinetic model for the adsorption of Ni^{2+} ions onto the (a) NaX and (b) NaY zeolites at different concentrations (pH ~7, adsorbent dose = 1 g/L and T = 298 K).

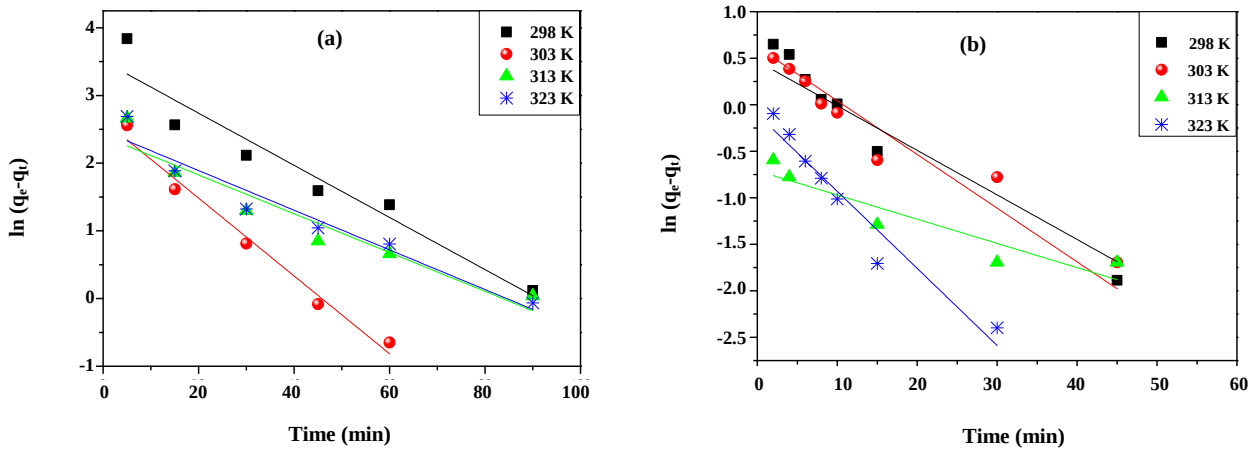

Fig. 8: Application of the Pseudo-First order kinetic model for the adsorption of Ni^{2+} ions onto the (a) NaX and (b) NaY zeolites at different Temperatures (pH ~7, C_i = 50 mg/L, adsorbent dose = 1 g/L).

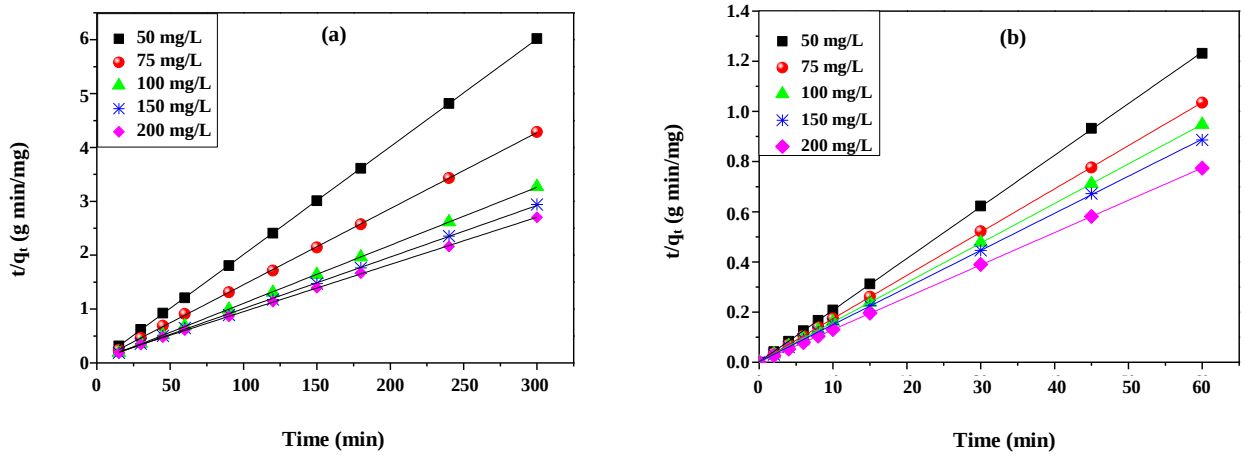

Fig. 9: Application of the pseudo-second order kinetic model for the adsorption of Ni^{2+} ions onto the (a) NaX and (b) NaY zeolites at different concentrations (pH ~7, C_i = 50 adsorbent dose = 1 g/L and T = 298 K).

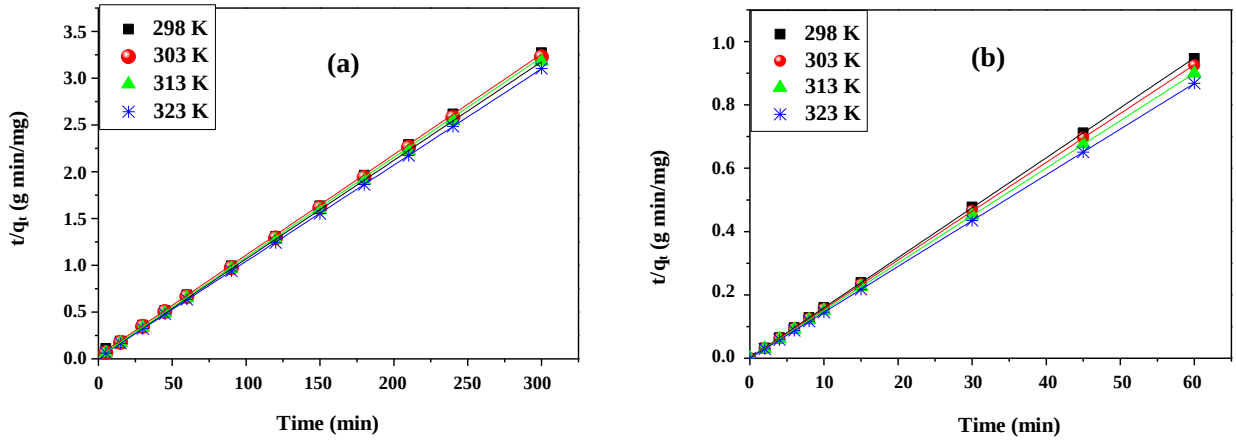

Fig. 10: Application of the pseudo-second order kinetic model for the adsorption of Ni^{2+} ions onto the (a) NaX and (b) NaY zeolites at different temperatures (pH ~7, C_i = 50 mg/L, adsorbent dose = 1 g/L).

these ions are pseudo second order. We also notice a decrease in the rate constant k_2 with the increase of the initial concentration of Ni^{2+} ions which can be explained by the solute-solute interactions. We also observe an increase in the constant of velocity k_2 as a function of the temperature which would indicate an increase of the interactions between the Ni^{2+} ions [52-54].

The good adaptation of the experimental results to the pseudo second order model suggest that the fixation of the Ni^{2+} ions on the two zeolites studied is mainly due to chemical adsorption. Indeed, Ho and McKay indicate that the adsorption kinetics of most metal ions on adsorbents are consistent with the hypothesis of the pseudo-second order model according to the metal ions interact with the different functional groups on the surface of the materials. Therefore we can conclude that the pseudo-second order model represents the experimental results, this model was often adopted to model the adsorption kinetics of heavy metals on both NaX and NaY zeolites [20, 22, 55].

Diffusion kinetics

External diffusion

The external diffusion is modeled starting from the Eq. (11) [55,56]. The variation of the concentration in aqueous solution in the liquid phase can be presented as follows:

Table 4: Pseudo (First, Second) Order adsorption rate constants and the correlation coefficient (R^2) values of Ni^{2+} ions onto NaX and NaY.

		Pseudo first ordre				Pseudo second ordre		
		$q_{e,\ exp}$ (mg/g)	$q_{e,\ cal}$ (mg/g)	$k_1\times10^2$ (min^{-1})	R^2	$q_{e,\ cal}$ (mg/g)	$k_2\times10^3$ (g/mg min)	R^2
NaX	C_o (mg/L)							
	50	49.48	6.740	5.368	0.6970	49.98	28.571	0.9998
	75	69.94	11.18	2.201	0.8964	71.43	5.078	0.9999
	100	91.71	21.81	3.181	0.9767	92.59	4.050	0.9999
	150	101.98	70.18	4.564	0.8138	104.17	1.786	0.9996
	200	111.00	38.61	1.878	0.9924	113.64	1.022	0.9998
	T(°C)							
	25	91.71	21.81	3.181	0.9767	92.59	4.050	0.9999
	30	92.92	13.90	5.747	0.9813	93.45	6.250	0.9999
	40	94.34	11.01	2.866	0.9195	95.24	8.891	0.9998
	50	96.64	11.90	2.930	0.9423	97.08	8.420	0.9997
NaY	C_o (mg/L)							
	50	48.70	1.009	2.000	0.8544	48.59	193.374	0.9999
	75	57.98	1.426	7.672	0.9920	58.00	199.640	0.9999
	100	63.35	1.858	5.7720	0.9656	63.37	136.154	0.9999
	150	67.72	2.976	6.604	0.9854	67.61	95.616	0.9999
	200	77.56	1.004	4.907	0.9471	77.57	137.35	0.9999
	T(°C)							
	25	63.13	1.858	5.772	0.9656	63.37	136.154	0.9999
	30	64.83	1.596	4.789	0.9384	64.85	157.69	0.9999
	40	66.72	2.034	2.602	0.8193	66.53	468.43	0.9999
	50	69.11	1.107	8.286	0.9342	69.15	355.31	0.9999

$$V\frac{dC_t}{d_t} = -k_f S\left(C_t - C_s\right) \quad (11)$$

Where C_s (mg/L): concentration of the Ni^{2+} ions at the surface of the adsorbent; C_t (mg/L): Ni^{2+} concentration in the liquid phase at the time t; S (cm^2): exchange surface concerned with external diffusion; K_f (cm/s): external diffusion coefficient and V(L): volume of the solution. After integration of the equation (11) for the boundary conditions: $C_{s=}$ 0 and $C_{s=}$ C_i at t = 0 and $C_{t=}$ C_t, at t = t, we obtain the Equation (12):

$$\ln\left(\frac{C_t}{C_i}\right) = -k_f\left(\frac{S}{V}\right)t \quad (12)$$

In the case of spherical particles, the report $\left(\frac{S}{V}\right)$ takes the following form (13):

$$\left(\frac{S}{V}\right) = \frac{3F}{\rho d_p} \quad (13)$$

Where ρ is the density of the adsorbent (g/cm^3); F is adsorbent dose (g/L) and d_p(cm): average particle diameter. The external diffusion coefficient (k_f) is obtained from the slope of the linear curve ln (C_t/C_i) as a function of time. Fig.11 shows the linearization of the curve ln (C_t/C_i) as a function of time, which makes

Table 5: Values of external diffusion coefficient k_f, intra-particle diffusion rate constant k_{int}, intra-particle diffusion coefficients D_i and number of Biot (B_i) of Ni^{2+} ions adsorption onto NaX and NaY.

	$k_f \times 10^4$ (cm/s)	R^2	k_{int} (mg/g.min^{0,5})	R^2	$D_i \times 10^{11}$ (cm^2/s)	R^2	Bi	E_a (kJ/mol)
NaX	0.8981	0.9027	0.4164	0.9108	1.1285	0.9004	5570.84	38.95
NaY	0.2359	0.966	0.2051	0.9717	0.3706	0.902	4455.02	37.11

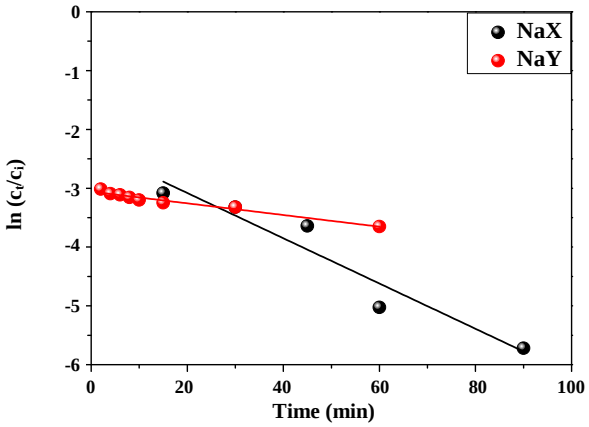

Fig. 11: Application of the external diffusion model for the adsorption of Ni^{2+} ions onto NaX and NaY (C_i = 50 mg/L, pH ~7, adsorbent dose = 1 g/L and T = 298 K).

it possible to calculate the external diffusion coefficient. The values of the external adsorption coefficients of Ni^{2+} ions onto NaX and NaY are grouped in Table 5.

From these results, we find that the correlation coefficients (R^2) obtained are relatively low for NaX and NaY. We also note that $\ln(C_t / C_i)$ plots as a function of time do not pass through the origin, which shows that the external diffusion is not the limiting step of the adsorption.

Intraparticle diffusion

Adsorption is a complex phenomenon, which generally follows a path involving the combination of surface adsorption and diffusion in the pores**.** The extension of a particulate diffusion to the total process can be evaluated by the Weber and Morris model Equation (14). This model was chosen, assuming that the rate of adsorption in the porous adsorbents is often controlled by transport in the pores. The Weber and Morris model shows that surface adsorption is predominant whereas that in the pores is secondary.

$$q_t = k_{int} t^{1/2} + C \qquad (14)$$

Where k_{int} (mg/g $min^{1/2}$): intraparticle diffusion rate constant; *C* (parameter of Weber and Morris); The constant k_{int} is deduced from the slope of the linear part of the curve (q_t) as a function of $t^{1/2}$.

The Weber and Morris scattering model were applied for the determination of intra particle diffusion rate constants, the description of the experimental results of the adsorption kinetics by this model is presented in the Fig.12.

According to the results, the modeling of intra-particle diffusion characterized by the Weber-Morris relation between the adsorbed quantity q_t and time t present a multi-linearity, showing an evolution in the adsorption process. Indeed, the first step is very short, corresponds to a limitation of the adsorption by external diffusion. While the second step corresponds to the progressive adsorption of the solute, the phenomenon being then limited by the intraparticle diffusion. The third stage characterized by a plateau corresponds of a state of equilibrium [57]. The values of the intra particle diffusion rate constants for the adsorption of the Ni^{2+} ions onto NaX and NaY are grouped in the Table 5. It is important to note that the intra-particle diffusion constant rate of the NaX is greater than that of the NaY.

Intra -particle diffusion coefficient

In this study Fick's law model for intra-particular diffusion were applied the initial diffusion coefficients Di, were calculated from the following equations (15):

$$\frac{q_t}{q_e} = 1 - \frac{6}{\pi^2} \sum_{n=1}^{\infty} \frac{1}{n^2} \exp\left(-\frac{D n^2 \pi^2 t}{r_o^2}\right) \qquad (15)$$

where q_t/q_e, t, r_0 and n are the fractional attainment of equilibrium at time of amounts of adsorption, time, radius of crystalline particles assumed to be spherical, and an integer respectively. In short time, Equation (15) can be rearranged to obtain Eq. (16) [6, 25, 58]. Similar model is developed for the determination of the intra-particle diffusion coefficient (Eq (17)).

$$\frac{q_t}{q_e} = \frac{6}{r_o}\left(\frac{D_i t}{\pi}\right)^{1/2} \qquad (16)$$

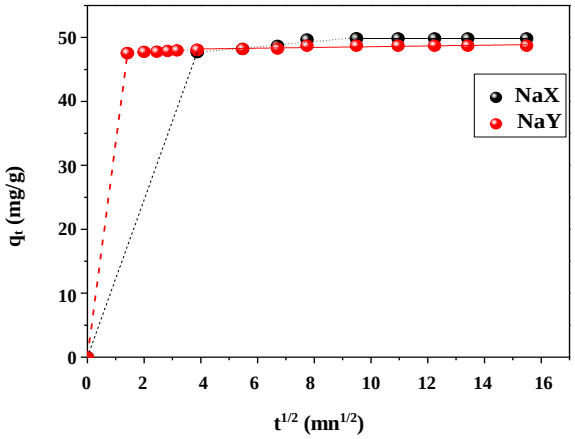

Fig. 12: Application of the intraparticle diffusion kinetic model for the adsorption of Ni^{2+} ions onto NaX and NaY (C_i = 50 mg/L, pH ~7, adsorbent dose = 1 g/L and T = 298 K).

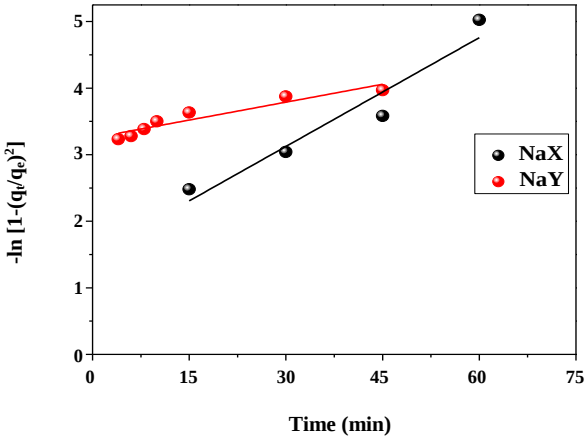

Fig. 13: Intraparticle diffusion pattern of Ni^{2+} ions adsorption onto NaX and NaY (C_i = 50 mg/L, pH ~7, adsorbent dose = 1 g/L and T = 298 K).

$$-\ln\left[1-\left(\frac{q_t}{q_e}\right)^2\right]=\left(\frac{4\pi^2 D_i}{d_p^2}\right)t \qquad (17)$$

Where D_i and d_p denote the intraparticle diffusion coefficient (cm^2/s) and the average particle diameter (cm) respectively. The initial diffusion coefficients D_i are obtained from plots of $-\ln\left[1-\left(\frac{q_t}{q_e}\right)^2\right]$ vs t (Fig. 13). In this study, q_∞ value is represented by q_e for our adsorption experiment of Ni^{2+} ions by both NaX and NaY samples.

From the results obtained in Table 5, we note that the intra-particle diffusion coefficients are lower than those of the external diffusion coefficients .Therefore, it can be concluded that adsorption kinetics are controlled by intra-particle diffusion model.

The diffusion coefficient value of Ni^{2+} ions onto our adsorbent show that the diffusion of NaX sample was better than NaY due to the diameter pore. Based on previous work, the calculation of the Biot number made it possible to determine the limiting diffusion mechanism. If this number is greater than 100, the resistance due to the transfer of external matter is negligible in front of that due to the internal transfer. We note that the transfer of matter is controlled by the latte. On the other hand, if this number is less than 100, The resistance due to the transfer of external material becomes the limiting step [56].

The number of Biot (B_i) dimensionless is given by the following formula Eq (18):

$$Bi=\frac{k_f \times d_p}{D_i} \qquad (18)$$

Where k_f, D_i and d_p denote respectively the external diffusion coefficient, the intra particle diffusion coefficient and the particle diameter.

The intra-particle diffusion coefficients, the external diffusion coefficients and the Biot numbers for the adsorption of the Ni^{2+} ions on the NaX and NaY are grouped in the Table 5. From the results, we observe that the number of Biot (Bi) is much greater than the value 100, which confirms that the limiting step is the intra particle diffusion.

Activation Energy

The activation energy is a criterion of distinction between chemical adsorption and physical adsorption, which is calculated from the Arrhenius law:

$$K_2=A_o \exp\left(\frac{-E_a}{RT}\right) \qquad (19)$$

Where K_2 (g/mg.min): pseudo second order adsorption rate constant, A_o (g/mg.min): temperature independent factor, E_a (kJ/mol): activation energy of adsorption, R (8.314 J/mol.K): molar gas constant and T (K): absolute temperature. After linearization of Eq. (19), we obtain Eq. (20) [59].

$$\ln k_2=\ln A_o-\frac{E_a}{RT} \qquad (20)$$

Table 6: Thermodynamic Parameters of Ni^{2+} ions adsorption onto NaX and NaY.

	ΔH^o (kJ/mol)	ΔS^o (J/mol K)	ΔG^o (kJ/mol)			
			298 K	303 K	313 K	323 K
NaX	29.437	175.883	-22.976	-23.855	-25.614	-27.373
NaY	8.055	31.584	-1.360	-1.519	-1.835	-2.151

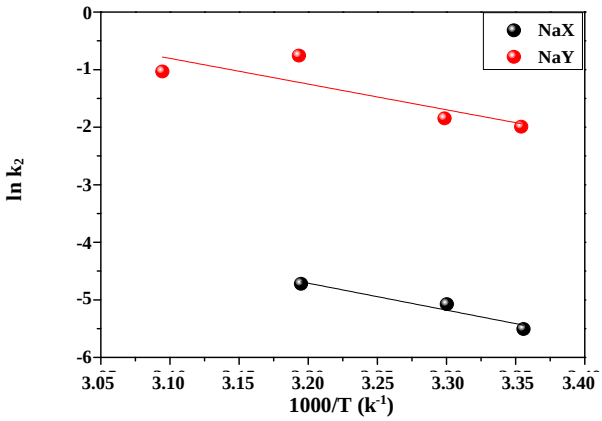

Fig. 14: Characteristic Curves of Arrhenius for the adsorption of Ni^{2+} ions onto the NaX and NaY zeolites Temperatures (pH ~7, Co = 50 mg/L, adsorbent dose = 1 g/L).

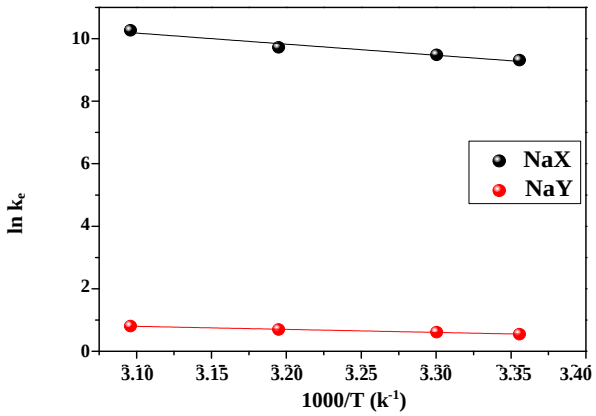

Fig. 15: Variation of ln K_c as a Function of (1/T): NaX and NaY Zeolite Temperatures (pH ~7, C_i = 50 mg/L, adsorbent dose = 1 g/L).

By plotting (ln k_2) as a function of (1/T). Determining the activation energy (E_a). Activation energies of the adsorption of Ni^{2+} ions onto NaX and NaY are summarized in Table 5. From these results, we note that the activation energy values obtained during this study for the adsorption of ions Ni^{2+} onto NaX and NaY are less than 40 kJ/mol. The results show that the adsorption process follows a chemical nature (Fig. 14).

Thermodynamic Parameters

The thermodynamic parameters of the adsorption process, free energy (ΔG°), enthalpy (ΔH°) and the entropy (ΔS°) explain the mechanism of the Ni (II) ions adsorption onto NaX and NaY. The variation of the enthalpy (ΔH^o) and the entropy (ΔS^o) can be obtained from the slope and the interception of the ln K_c plot as a function of (1/T) (Fig.15).

The values of thermodynamic parameters are listed in Table 6. The free Gibbs enthalpy of adsorption is calculated by the following equation (22):

$$\ln k_c = \left(\frac{\Delta S^\circ}{R}\right) - \left(\frac{\Delta H^\circ}{RT}\right) \quad (21)$$

$$\Delta G^\circ = \Delta H^\circ - T\Delta S^\circ \quad (22)$$

The analysis of these thermodynamic parameters reveals that the adsorption of Ni^{2+} ions is a spontaneous reaction (ΔG°< 0). The decrease of ΔG° with the increase of the temperature shows that the adsorption is more suitable to high temperature. The values of the entropy variables of the adsorption of Ni^{2+} ions are positive which means that the molecules in the liquid phase and reflect the great affinity of the adsorbent materials NaX and NaY toward Ni(II) ions [20]. The adsorption of Ni(II) ions and water molecules in the zeolite framework to replace Na^+ ions contributed to the increasing of the entropy [60]. The ΔH° values show that adsorption process is endothermic.

Comparative adsorption capacities onto other material adsorbents

The maximum Nickel (II) adsorption capacity, according to the Langmuir model shows that the both zeolites NaX and NaY have high potentials compared to others adsorbents tested in several Langmuir Ni^{2+} adsorption research. Table 7 shows the maximum ions capacity comparison of several adsorbents. It is clear

Table 7: Comparison of maximum adsorption capacities of Ni^{2+} ions by various adsorbents.

Adsorbents	q_m (mg/g)	Ref.
Natural zeolite	8.69	[62]
Na-zeolite	1.30	[63]
Escherichia coli biofilm supported on zeolite NaY	13	[64]
kinetic and thermodynamics of nickel removal	10.1	[65]
citrus limettioides peel and seed carbon (CLSC)	35.54	[66]
NaX	111.85	This work
NaY	77.57	This work

Table 8: Some physico-chemical properties of the wastewater from effluent issued from the industrial zone (West Algiers, Algeria).

Physicochemical parameters	Zeolite	
	NaX	NaY
Initial pH	7	7
Final pH	7.5	7.41
Initial Conductivity (mS/cm)	2.5	2.5
Final Conductivity (mS/cm)	0.82	0.85
Ni^{2+} Removal (%)	77.81	83.86

that both zeolites NaX and NaY show significantly better performance than the others adsorbents.

Treatment of nickel (II) wastewater

Nickel (II) wastewater samples have been taken from effluent issued from the industrial zone in West (Algiers), some physico-chemical properties were obtained and illustrated in Table 8. Then, adsorption Ni^{2+} tests have been carried out onto NaX and NaY zeolites using optimal conditions previously determined.

It has been found that the Ni^{2+} removal yield was 83.86% and 77.81% for NaX and NaY respectively. Comparing the removal efficiencies (percentage) for zeolites, Table 8 shows that the NaX performs considerably better than the NaY. Moreover, NaX have small particles with an average size of 4 and 3 µm. These characteristics allow the Ni^{2+} ions to access and diffuse in the framework structures [61] (Fig. 16).

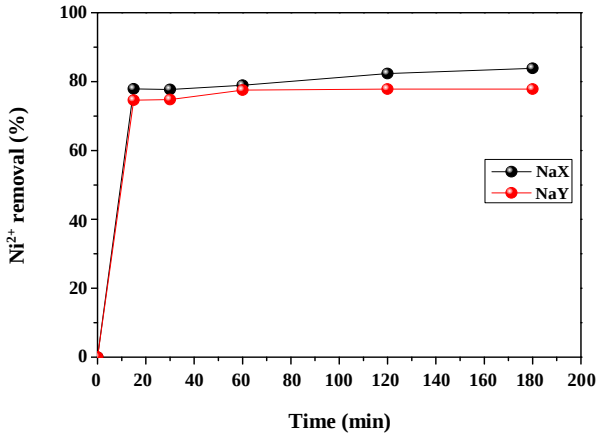

Fig. 16: Treatment of Ni^{2+} wastewater with NaX and NaY zeolites (pH ~7, C_i= 50 mg/L, adsorbent dose = 1 g/L and T = 298K).

CONCLUSIONS

In this work we successfully prepared two adsorbents NaX and NaY zeolites by hydrothermal method. The characterization results indicate that the zeolites are obtained with high crystalline structure and good morphology.

The yield of adsorption appears to be strongly influenced by some parameters such as pH, temperature, solid/liquid ratio and the initial concentration of the metal ion. Indeed, the obtained results showed that at low pH, the elimination yield is relatively low. This could be

explained by competition of Ni^{2+} and H^{+} at the adsorbent sites. The optimum pH to eliminate Ni^{2+} ions using our adsorbents are in the range of 6 -7. The diffusion coefficient decreases both for NaX and NaY with increasing the concentration of Ni^{2+} ions point out that less favorable media take part when effluent concentration increases. The adsorption isotherm study is represented very correctly by the Langmuir model with maximum adsorption capacity varying from 77 to 120 mg /g for Ni^{2+} ions. Analysis of experimental kinetic data has shown that the pseudo second order model well describes the adsorption. The study of the diffusion mechanisms of Ni^{2+} ions adsorption indicate that intra particle diffusion is the limiting step of the process. The positive value of ΔH^{o} and ΔS^{o} related to the adsorption process of Ni^{2+} ions onto the NaX and NaY zeolites showed that the process is endothermic and spontaneous. All optimized parameters have been applied on algerian industrial wastewater solution and the Ni^{2+} removal yield was 83.86 and 77.81 % for NaX and NaY zeolites respectively. These encouraging results lead us to future large-scale application.

Received : Feb. 4, 2018 ; Accepted : Sep. 24, 2018

REFERENCES

[1] Mekatel H., Amokrane S., Benturki A., Nibou D., Treatment of Polluted Aqueous Solutions by Ni^{2+}, Pb^{2+}, Zn^{2+}, Cr^{+6}, Cd^{2+} and Co^{2+} Ions by Ion Exchange Process Using Faujasite Zeolite, *Proc. Eng.*, **33**: 52–57 (2012).

[2] Nibou D., Amokrane S., Catalytic Performances of Exchanged Y Faujasites by Ce^{3+}, La^{3+}, UO_2^{2+}, Co^{2+}, Sr^{2+}, Pb^{2+}, Tl^{+} and NH_4^{+} Cations in Toluene Dismutation Reaction, *Compt. Rend. Chim.*, **13**(5): 527-537 (2010).

[3] Tan P., Hu Y., Bi Q., Competitive Adsorption of Cu^{2+} Cd^{2+} and Ni^{2+} from an Aqueous Competitive Adsorption of Cu^{2+}, Cd^{2+} and Ni^{2+} from an Aqueous Solution on Graphene Oxide Membranes, *Colloid Surface A.*, **509**: 56-64 (2016).

[4] Nezamzadeh-Ejhieh A., Shahanshahi M., Modification of Clinoptilolite Nano-Particles with *hexadecylpyridinium* Bromide Surfactant as an Active Component of Cr (VI) Selective Electrode, *J. Ind. Eng. Chem.*, **19**(6): 2026-2033 (2013).

[5] Derikvandi, H., Nezamzadeh-Ejhieh A., Increased Photocatalytic Activity of NiO and ZnO in Photodegradation of a Model Drug Aqueous Solution: Effect of Coupling, Supporting, Particles Size and Calcination Temperature, *J. Hazard. Mater.*, **321**: 629-638 (2017).

[6] Nibou D., Mekatel H., Amokrane S., Barkat M., Trari M., Adsorption of Zn^{2+} Ions onto NaA and NaX Zeolites: Kinetic, Equilibrium and Thermodynamic studies, *J. Hazard. Mater.*, **173**: 637-646 (2010).

[7] Aid A., Amokrane S., Nibou D., Mekatel E., Trari M., Hulea V., Modeling Biosorption of Cr (VI) onto Ulva Compressa L. from Aqueous Solutions, *Wat. Sci. Tech.*, **77** (**1**), 60-69 (2018).

[8] Esmaeili N., Kazemian H., Bastani D., Synthesis of Nano Particles of LTA Zeolite by Means of Microemulsion Technique, *Iran. J. Chem. Chem. Eng. (IJCCE)*, **30**.2: 1-8 (2011).

[9] Esmaeili N., Kazemian H., Bastani D., Controlled Crystallization of LTA Zeolitic Nanoparticles from a Clear Solution Using Organic Template, *Iran. J. Chem. Chem. Eng. (IJCCE)*, **30**.2: 9-14 (2011).

[10] Tosheva L., Valentin P.V., Nanozeolites: Synthesis, Crystallization Mechanism, and Applications, *Chem. Mater.*, **17**(10): 2494-2513 (2005).

[11] Nezamzadeh-Ejhieh A., Shahriari E., Photocatalytic Decolorization of Methyl Green Using Fe (II)-o-Phenanthroline as Supported onto Zeolite Y, *J. Ind. Eng. Chem.*, **20**.5: 2719-27 (2014).

[12] Krobba A., Nibou D., Amokrane S., Mekatel H., Adsorption of Copper (II) onto Molecular Sieves NaY, *Desal. Wat. Treat.*, **37**: 1–7 (2012).

[13] Amokrane S., Rebiai R., Nibou D., Behaviour of Zeolite A, Faujasites X and Y Molecular Sieves in Nitrogen Gas Adsorption, *J. Appl. Sci.*, **7**: 1985-1988 (2007).

[14] Breck D.W., "Zeolite Molecular Sieves-Structure Chemistry and Use", Wiley Interscience, New York (1974).

[15] Nezamzadeh-Ejhieh A., Khorsandi M., Hotodecolorization of Eriochrome Black T Using NiS–P Zeolite as a Heterogeneous Catalyst, *J. Hazard. Mater.*, **176**(1-3): 629-637 (2010)

[16] Nezamzadeh-Ejhieh A., Khorsandi S., Photocatalytic Degradation of 4-nitrophenol with ZnO Supported Nano-Clinoptilolite Zeolite, *J. Ind. Eng. Chem.* **20**(3): 937-946 (2014).

[17] Mahdavi M., Nezamzadeh-Ejhieh A., An aluminum Selective Electrode via Modification of PVC Membrane by Modified Clinoptilolite Nanoparticles with Hexadecyltrimethyl Ammonium Bromide (HDTMA-Br) Surfactant Containing Arsenazo III, *J. Colloid interf. Sci.*, **494**: 317-324 (2017).

[18] Sistani S., Ehsani M.R., Kazemian H., Microwave Assisted Synthesis of Nano Zeolite Seed for Synthesis Membrane and Investigation of its Permeation Properties for H_2 Separation, *Iran. J. Chem. Chem. Eng. (IJCCE)*, **29**(4): 99-104 (2010).

[19] Frising T., Leflaive P., Extraframework Cation Distributions in X and Y Faujasite Zeolites: A Review, *Mic. Mes. Mat.*, **114**: 27-63 (2008).

[20] Barkat M., Nibou D., Amokrane S., Chegrouche S., Mellah A., Uranium (VI) Adsorption on Synthesized 4A and P1 Zeolites: Equilibrium, Kinetic, and Thermodynamic Studies, *Com. Rend. Chim.*, **18**(**3**): 261-269 (2015).

[21] Barrer R., Zeolites and Clay Minerals as Sorbents and Molecular Sieves, Ed. Academic Press (1978).

[22] Houhoune F., Djamel N., Samira A., Mahfoud B., Modelling and Adsorption Studies of Removal Uranium (VI) Ions on Synthesised Zeolite NaY, *Des. Wat. Treat.*, **51** (**28-30**): 5583-5591(2013)

[23] Blanchard G., Maunaye M., Martin G., Removal of Heavy Metals from Waters by Means of Natural Zeolites, *Water. Res*, **18**: 1501-1507 (1984).

[24] Barkat M., Nibou D., Chegrouche S., Mellah A., Kinetics and Thermodynamics Studies of Chromium (VI) Ions Adsorption onto Activated Carbon from Aqueous Solutions, *Chem. Eng. Proc. Pro. Intens.*, **48** (1): 38-47 (2009).

[25] Beyond G., Adamson A., Myers L., The Exchange Adsorption of Ions from Aqueous Solutions by Organic Zeolites, *J. Am. Chem. Soc.*, **69**: 2836-2848 (1947).

[26] Turse R., Rieman III W., Kinetics of Ion Exchange in a Chelating Resin, *J. Phs. Chem.*, **65**: 1821-1824 (1961).

[27] Biškup B., Subotić B., Kinetic Analysis of the Exchange Processes between Sodium Ions from Zeolite A and Cadmium, Copper and Nickel Ions from Solutions, *Sep. Puri. Technol.*, **37**: 17-31 (2004).

[28] Sinha P., Panicker P., Amalraj R., Krishnasamy V., Treatment of Radioactive Liquid Waste Containing Caesium by Indigenously Available Synthetic Zeolites: A Comparative Study, *Waste. Manage.*, **15**: 149-157 (1995).

[29] Aid A., Amokrane S., Nibou D., Mekatel H., Removal of Cr^{6+}, Co^{2+} and Ni^{2+} Ions from Aqueous Solutions by Algerian Enteromorpha Compressa (L.) Biomass, *World Academy of Science, Engineering and Technology, Inter. J. Ecol. Eng.*, **11**(7): - (2017).

[30] Mekatel H., Amokrane S., Bellal B., Trari M., Nibou D., Photocatalytic Reduction of Cr (VI) on Nanosized Fe_2O_3 Supported on Natural Algerian Clay: Characteristics, Kinetic and Thermodynamic Study, *Chem. Eng. J.*, **200:** 611-618 (2012).

[31] Baerlicher C., Meier W.M., Olson D.H., "Atlas of Zeolite Fromewerk Types", 5th Revised Ed., Elsevier, Amesterdam (2001).

[32] Khodadadi, B., Bordbar M., Sonochemical Synthesis of Undoped and Co-Doped ZnO Nanostructures and Investigation of Optical and Photocatalytic Properties, *Iran. J. Catal.*, **6**(1): 37-42 (2016).

[33] Nezamzadeh-Ejhieh, A., Afshari E., Modification of a PVC-Membrane Electrode by Surfactant Modified Clinoptilolite Zeolite Towards Potentiometric Determination of Sulfide, *Micro. Meso. Mater.*, **153**: 267-274 (2012).

[34] Nezamzadeh-Ejhieh A., Badri A., Application of Surfactant Modified Zeolite Membrane Electrode Towards Potentiometric Determination of Perchlorate, *J. Electroanal. Chem*. **660**(1): 71-79 (2011).

[35] Nezamzadeh-Ejhieh A., Badri A., Surfactant Modified ZSM-5 Zeolite as an Active Component of Membrane Electrode Towards Thiocyanate, *Desalination*, **281**: 248-256 (2011).

[36] Mekatel EH., Amokrane S., Aid A., Nibou D., Trari M., Adsorption of Methyl Orange on Nanoparticles of a Synthetic Zeolite NaA/CuO, *Com. Rend. Chim.*, **18**(3), 336-344 (2015).

[37] Senobari S., Nezamzadeh-Ejhieh A., A Comprehensive Study on the Enhanced Photocatalytic Activity of CuO-NiO Nanoparticles: Designing the Experiments, *J. Mol. Liq.*, **261**: 208-217 (2018).

[38] Anari-Anaraki, M., Nezamzadeh-Ejhieh A., Modification of an Iranian Clinoptilolite Nano-Particles by Hexadecyltrimethyl Ammonium Cationic Surfactant and Dithizone for Removal of Pb (II) from Aqueous Solution, *J. Colloid. Interf. Sci.*, **440**: 272-281 (2015).

[39] Nibou D., Amokrane S., Lebaili N., Use of NaX Porous Materials in the Recovery of Iron Ions, *Desalination* **250** (**1**): 459-462 (2010).

[40] Borandegi M., Nezamzadeh-Ejhieh A., Enhanced Removal Efficiency of Clinoptilolite Nano-Particles Toward Co (II) from Aqueous Solution by Modification with Glutamic Acid, *Colloids Surf. A: Physicochem. Eng. Aspects* **479**: 35-45 (2015).

[41] Garba Z.N., Ugbaga N.I., Abdullahi A.K., Evaluation of Optimum Adsorption Conditions for Ni (II) and Cd (II) Removal from Aqueous Solution by Modified Plantain Peels (MPP), *Beni-Suef Univ. J. Basic Appl. Sci.*, **5**: 170-179 (2016).

[42] Marcos C., Rodríguez I., Thermoexfoliated Commercial Vermiculites for Ni^{2+} Removal, *Appl. Clay. Sci.*, **132**: 685-693 (2016).

[43] Fakari S., Nezamzadeh-Ejhieh A., Synergistic Effects of ion Exchange and Complexation Processes in Cysteine-Modified Clinoptilolite Nanoparticles for Removal of Cu (II) from Aqueous Solutions in Batch and Continuous Flow Systems, *New J. Chem.* **41**(10): 3811-3820 (2017).

[44] Eshraghi F., Nezamzadeh-Ejhieh A., EDTA-Functionalized Clinoptilolite Nanoparticles as an Effective Adsorbent for Pb (II) Removal, *Environ. Sci. Pol. Res.*, **25**(14): 14043-14056 (2018).

[45] Lamgmuir I., The Constitution and Fundamental Properties of Solids and Liquids, Part 1. Solids, *J. Am. Chem. Soc.*, **38**: 2221-2295 (1916).

[46] Freundlich H., Uber die Adsorption in Losungen [Adsorption in Solution], *Z. Phys. Chem.*, **57:** 385–470 (1906).

[47] Temkin M.I., Adsorption Equilibrium and the Kinetics of Processes on Nonhomogeneous Surfaces and in the Interaction between Adsorbed Molecules, *Zh. Fiz. Chim*, **15**: 296-332 (1941).

[48] Nezamzadeh-Ejhieh A., Kabiri-Samani M., Effective Removal of Ni (II) from Aqueous Solutions by Modification of Nano Particles of Clinoptilolite with Dimethylglyoxime, *J. Hazard. Mater.*, **260**: 339-349 (2013).

[49] Heidari-Chaleshtori M., Nezamzadeh-Ejhieh A., Clinoptilolite Nano-Particles Modified with Aspartic Acid for Removal of Cu (II) from Aqueous Solutions: Isotherms and Kinetic Aspects, *New J. Chem*. **39**.12: 9396-9406 (2015).

[50] Ghasemi M., Javadian H., Ghasemi N., Agarwal S.,. Gupta V.K., Microporous Nanocrystalline NaA Zeolite Prepared by Microwave Assisted Hydrothermal Method and Determination of Kinetic, Isotherm and Thermodynamic Parameters of the Batch Sorption of Ni (II), *J. Mol. Liq.*, **215**: 161-169 (2016).

[51] Fritzsche S., Haberlandt R., Jost S.,. Schüring A., Modelling Diffusion in Zeolites by Molecular Dynamics Simulations, *Mol. Simulat.*, **25**: 27-40 (2000).

[52] Dissanayake D., Wijesinghe W., Iqbal S., Priyantha N., Iqbal M., Isotherm and Kinetic Study on Ni (II) and Pb (II) Biosorption by the Fern Asplenium Nidus L, *Ecol. Eng.*, **88**: 237-241 (2016).

[53] Naghash A., Nezamzadeh-Ejhieh A., Comparison of the Efficiency of Modified Cinoptilolite with HDTMA and HDP Surfactants for the Removal of Phosphate in Aqueous Solutions, *J. Ind. Eng. Chem.* **31**: 185-191 (2015).

[54] Shirzadi H., Nezamzadeh-Ejhieh A., An Efficient Modified Zeolite for Simultaneous Removal of Pb (II) and Hg (II) from Aqueous Solution, *J. Mol. Liq.*, **230**: 221-229 (2017).

[55] Tajiki, A., Abdouss, M., Synthesis and Characterization of Graphene Oxide Nano-Sheets for Effective Removal of Copper Phthalocyanine from Aqueous Media, *Iran. J. Chem. Chem. Eng. (IJCCE)*, **36**(4): 1-9 (2017).

[56] Yousefpour M., Modelling of Adsorption of Zinc and Silver Ions on Analcime and Modified Analcime Zeolites Using Central Composite Design, *Iran. J. Chem. Chem. Eng. (IJCCE)*, **36** (4): 81-90 (2017).

[57] Wu F.C., Tseng R.L., Juang R.S., Initial Behavior of Intraparticle Diffusion Model Used in the Description of Adsorption Kinetics, *Chem. Eng. J*, **153**: 1-8 (2009).

[58] Martins L.F., Parreira M.C.B., Ramalho J.P.P., Morgado P., Filipe E.J., Prediction of Diffusion Coefficients of Chlorophenols in Water by Computer Simulation, *Fluid Phase Equilibr*, **396**: 9-19 (2015).

[59] Nuhoglu Y., Malkoc E., Thermodynamic and Kinetic Studies for Environmentaly Friendly Ni (II) Biosorption Using Waste Pomace of Olive Oil Factory, *Bioresource Technol* **100**: 2375-2380 (2009).

[60] Wu Y., Wang L., Kinetic and Thermodynamic Studies of the Biosorption of Ni (II) by Modified Rape Straw, *Procedia Environ Sci.*, **31**: 75-80 (2016).

[61] Pitcher S., Slade R., Ward N., Heavy Metal Removal from Motorway Stormwater Using Zeolites, *Sci. Total Environ.*, **334**: 161-166 (2004).

[62] Çoruh S., Ergun O.N., Ni^{2+} Removal from Aqueous Solutions Using Conditioned Clinoptilolites: Kinetic and Isotherm Studies, *Environmental Progress & Sustainable Energy* **28**: 162-172 (2009).

[63] Turkman A., Aslan S., Ege I., Treatment of Metal Containing Wastewaters by Natural Zeolites, *Fresen. Environ. Bull*, ***13***: 574-580 (2004).

[64] Quintelas C., Rocha Z., Silva B., Fonseca B., Figueiredo H., Tavares T., Biosorptive Performance of an Escherichia Coli Biofilm Supported on Zeolite NaY for the Removal of Cr (VI), Cd (II), Fe (III) and Ni (II), *Chem. Eng. J.*, **152**: 110-115 (2009).

[65] Lam Y.F., Lee L.Y., Chua S.J., Lim S.S., Gan S., Insights into the Equilibrium, Kinetic and Thermodynamics of Nickel Removal by Environmental Friendly Lansium Domesticum Peel Biosorbent, *Ecotoxicol. Environ. Saf.*, **127**: 61-70 (2016).

[66] Sudha R., Srinivasan K., Premkumar P., Removal of Nickel (II) from Aqueous Solution Using Citrus Limettioides Peel and Seed Carbon, *Ecotoxicol. Environ. Saf.*, **117**: 115-123 (2015).